Rational Reprogramming of the R2 Subunit of *Escherichia coli* Ribonucleotide Reductase into a Self-Hydroxylating Monooxygenase

Jeffrey Baldwin,[‡] Walter C. Voegtli,[§] Nelly Khidekel,[§] Pierre Moënne-Loccoz,[||] Carsten Krebs,[⊥] Alice S. Pereira,[⊥,†] Brenda A. Ley,[‡] Boi Hanh Huynh,[⊥] Thomas M. Loehr,[||] Pamela J. Riggs-Gelasco,[#] Amy C. Rosenzweig,[§] and J. Martin Bollinger, Jr.*[,‡]

Contribution from the Department of Biochemistry and Molecular Biology, Pennsylvania State University, University Park, Pennsylvania 16802, Department of Biochemistry, Molecular Biology, and Cell Biology and Department of Chemistry, Northwestern University, Evanston, Illinois 60208, Department of Biochemistry and Molecular Biology, Oregon Graduate Institute of Science and Technology, Portland, Oregon 97006-8921, Department of Physics, Emory University, Atlanta, Georgia 30322, and Department of Chemistry and Biochemistry, College of Charleston, Charleston, South Carolina 29424

Received June 12, 2000

Abstract: The outcome of O_2 activation at the diiron(II) cluster in the R2 subunit of *Escherichia coli* (class I) ribonucleotide reductase has been rationally altered from the normal tyrosyl radical (Y122$^\bullet$)[1] production to self-hydroxylation of a phenylalanine side-chain by two amino acid substitutions that leave intact the $(histidine)_2$-$(carboxylate)_4$ ligand set characteristic of the diiron-carboxylate family. Iron ligand Asp (D) 84 was replaced with Glu (E), the amino acid found in the cognate position of the structurally similar diiron-carboxylate protein, methane monooxygenase hydroxylase (MMOH). We previously showed that this substitution allows accumulation of a μ-1,2-peroxodiiron(III) intermediate,[2,3] which does not accumulate in the wild-type (wt) protein and is probably a structural homologue of intermediate **P** ($\mathbf{H_{peroxo}}$) in O_2 activation by MMOH.[4] In addition, the near-surface residue Trp (W) 48 was replaced with Phe (F), blocking transfer of the "extra" electron that occurs in wt R2 during formation of the formally Fe(III)Fe(IV) cluster **X**.[5−7] Decay of the μ-1,2-peroxodiiron(III) complex in R2-W48F/D84E gives an initial brown product, which contains very little Y122$^\bullet$ and which converts very slowly ($t_{1/2} \sim 7$ h) upon incubation at 0 °C to an intensely purple final product. X-ray crystallographic analysis of the purple product indicates that F208 has undergone ϵ-hydroxylation and the resulting phenol has shifted significantly to become a ligand to Fe2 of the diiron cluster. Resonance Raman (RR) spectra of the purple product generated with $^{16}O_2$ or $^{18}O_2$ show appropriate isotopic sensitivity in bands assigned to O-phenyl and Fe−O-phenyl vibrational modes, confirming that the oxygen of the Fe(III)−phenolate species is derived from O_2. Chemical analysis, experiments involving interception of the hydroxylating intermediate with exogenous reductant, and Mössbauer and EXAFS characterization of the brown and purple species establish that F208 hydroxylation occurs during decay of the peroxo complex and formation of the initial brown product. The slow transition to the purple Fe(III)−phenolate species is ascribed to a ligand rearrangement in which μ-O^{2-} is lost and the F208-derived phenolate coordinates. The reprogramming to F208 monooxygenase requires both amino acid substitutions, as very little ϵ-hydroxyphenylalanine is formed and pathways leading to Y122$^\bullet$ formation predominate in both R2-D84E and R2-W48F.[2,7]

Structurally characterized members of the diiron-carboxylate family of oxidases and oxygenases include the R2 subunit of ribonucleotide reductase (R2, from *Escherichia coli*[8,9] and mouse[10]), the hydroxylase component of soluble methane monooxygenase (MMOH, from *Methylococcus capsulatus* Bath[11,12] and *Methylosinus trichosporium* OB3b[13]), and stearoyl acyl carrier protein Δ^9-desaturase (Δ9D, from castor seed[14]). These proteins have similar tertiary structures[15,16] and contain nearly identical $(histidine)_2(carboxylate)_4$-coordinated dinuclear iron clusters, which function in reductive activation of O_2.[17−21] Despite these similarities, the outcomes of their reactions with O_2 range from alkane hydroxylation in MMOH,[18] to fatty acid

* Address correspondence to this author. E-mail: jmb21@psu.edu
‡ Pennsylvania State University.
§ Northwestern University.
|| Oregon Graduate Institute of Science and Technology.
⊥ Emory University.
† Present address: Departamento de Química, Faculdade de Ciências e Tecnologia, Universidade Nova de Lisboa, 2825 Monte de Caparica, Portugal.
# College of Charleston.

(1) Abbreviations used: R2, R2 subunit of ribonucleotide reductase; Y122$^\bullet$, neutral tyrosyl radical in R2 derived from one-electron oxidation of tyrosine number 122; MMOH, hydroxylase component of methane monooxygenase; **P**, the putative peroxodiiron(III) complex that accumulates during O_2 activation by MMOH; **X**, the formally Fe(III)Fe(IV) cluster that accumulates during oxygen activation by R2; RR, resonance Raman; EXAFS, extended X-ray absorption fine structure; Δ9D, stearoyl acyl carrier protein Δ^9 desaturase; wt, wild-type; equiv, equivalents; HEPES, 4-(2-hydroxyethyl)-1-piperazineethanesulfonic acid; EMTS, ethyl mercurithiosalicylic acid; MES, 2-(*N*-morpholino)ethanesulfonic acid; PEG, poly(ethylene glycol); δ, Mössbauer isomer shift; ΔE_Q, quadrupole splitting parameter; GC/MS, gas chromatography/mass spectrometry; $W^{+\bullet}$, tryptophan cation radical; **Q**, the formally diiron(IV) intermediate that accumulates during O_2 activation by MMOH and is thought to hydroxylate methane.

(2) Bollinger, J. M., Jr.; Krebs, C.; Vicol, A.; Chen, S.; Ley, B. A.; Edmondson, D. E.; Huynh, B. H. *J. Am. Chem. Soc.* **1998**, *120*, 1094−1095.

10.1021/ja002114g CCC: $20.00
Published on Web 06/29/2001

desaturation in Δ9D,[19] to formation of a stable tyrosyl radical by one-electron oxidation of an endogenous tyrosine residue in R2.[22] An understanding of the structural basis for the "tuning" of the (histidine)$_2$(carboxylate)$_4$-diiron unit for this array of reactions might impact current efforts to develop biomimetic diiron catalysts. It should also permit the reprogramming of the reactivity of a given diiron protein by modification of its structure through site-directed mutagenesis or other protein engineering methods. Conversely, the ability to rationally alter reactivity should be considered a criterion for demonstrating true understanding of the structural determinants thereof.

Sjöberg, Nordlund, and co-workers contributed two studies in which the outcome of the *E. coli* R2 reaction was altered from the normal one-electron oxidation of Y122 to hydroxylation of a different residue. In the first, phenylalanine (F) 208, which is close to the diiron center and is part of a hydrophobic "pocket" that surrounds the Y122$^{\bullet}$, was replaced with Y, and the resulting protein was shown to undergo primarily ϵ-hydroxylation of the Y208 side chain upon reaction with O_2.[23−25] In the second, replacement of cluster ligand glutamate (E) 238 with alanine was shown to alter the reaction outcome to primarily ϵ-hydroxylation of F208, with the resulting ϵ-hydroxyphenylalanine side chain becoming coordinated by an Fe ion of the cluster.[26] These seminal studies established the ability of the R2 active site to support a two-electron oxidation outcome and identified residue 208 as a target for the altered reactivity. More importantly, the potential for detailed mechanistic characterization of these R2 variants to yield insight into the divergent tuning of diiron cluster reactivity by the natural proteins seemed very high. Unfortunately, this potential has gone largely unfulfilled, as detailed understanding of the reaction mechanisms has not been forthcoming. Our own efforts in this regard have been hindered by our failure to identify reaction conditions under which oxidized diiron intermediates accumulate. In our hands, the diiron(II) clusters of both proteins react with O_2 much less rapidly than does the cluster of wild-type R2 (unpublished data), a condition that disfavors accumulation of intermediates. Thus, the extent to which the mechanism of either reaction is similar to that of an authentic diiron monooxygenase such as MMOH remains unknown. Indeed, in perhaps the most important mechanistic observation on these reactions to date, it was shown that the O-atom transferred to Y208 in the R2-F208Y reaction originates from H_2O rather than O_2.[27] This result allows for the possibility that the hydroxylation proceeds by sequential one-electron oxidations of the Y208 phenol and subsequent hydration of the carbocation rather than by an O-atom transfer mechanism, as one would expect of a monooxygenase. For hydroxylation of F208 in the R2-E238A reaction, it seems very likely that an O-atom transfer mechanism *is* operant, but this possibility has not been verified experimentally. Further motivation for the present study was our concern that, even if the structural and mechanistic bases for the effects of the F208Y and E238A substitutions on the R2 reaction outcome were to be elucidated, neither mutagenesis experiment could be considered to have recapitulated the divergent tuning of the (histidine)$_2$(carboxylate)$_4$-diiron unit by the natural proteins (R2, MMOH, and Δ9D), for the simple reason that neither variant contains the conserved ligand set. In R2-F208Y, the phenol side chain introduced by mutagenesis (the target of the hydroxylation) is a ligand to Fe1 in the diiron(II) reactant form,[26] whereas the natural proteins are devoid of phenol ligands.[15,21] R2-E238A lacks a carboxylate ligand that bridges the Fe(II) ions in the reactant state of wild-type R2.[28] MMOH and Δ9D also have E residues at the corresponding positions,[11,14] and their carboxylates are also bridging ligands in the reactant clusters.[12,14] It is evident that introduction of ligands not present in the natural proteins (the Y208 phenol) or removal of conserved ones (E238) could alter cluster reactivity in ways that might not be relevant to the tuning of reactivity by the natural proteins with their conserved ligand set.

In this work, we have sought to more accurately recapitulate Nature's tuning of the (histidine)$_2$(carboxylate)$_4$-diiron unit by engineering an R2 variant (R2-W48F/D84E) that mediates a two-electron oxidation outcome but retains the conserved ligand set. Structural and mechanistic studies have revealed that, like the aforementioned R2-E238A, R2-W48F/D84E also undergoes self-hydroxylation at the ϵ-carbon of F208Y upon reaction of its diiron(II) cluster with O_2. In addition, the results show that a stoichiometric quantity of a MMOH-like intermediate (the previously characterized μ-1,2-peroxodiiron(III) complex[3]) accumulates on the pathway to F208 hydroxylation and that the reaction proceeds by an O-atom transfer mechanism that one expects of a "true" monooxygenase. As this variant protein has been *designed* to have a two-electron oxidation outcome on the basis of specific structural and mechanistic rationales (described in the Discussion section), the confirmation of a hydroxylation outcome by an oxygen transfer mechanism provides support

(3) Moënne-Loccoz, P.; Baldwin, J.; Ley, B. A.; Loehr, T. M.; Bollinger, J. M., Jr. *Biochemistry* **1998**, *37*, 14659−14663.
(4) Liu, K. E.; Wang, D.; Huynh, B. H.; Edmondson, D. E.; Salifoglou, A.; Lippard, S. J. *J. Am. Chem. Soc.* **1994**, *116*, 7465−7466.
(5) Parkin, S. E.; Chen, S.; Ley, B. A.; Mangravite, L.; Edmondson, D. E.; Huynh, B. H.; Bollinger, J. M., Jr. *Biochemistry* **1998**, *37*, 1124−1130.
(6) Baldwin, J.; Krebs, C.; Ley, B. A.; Edmondson, D. E.; Huynh, B. H.; Bollinger, J. M., Jr. *J. Am. Chem. Soc.* **2000**, *122*, 12195−12206.
(7) Krebs, C.; Chen, S.; Baldwin, J.; Ley, B. A.; Patel, U.; Edmondson, D. E.; Huynh, B. H.; Bollinger, J. M., Jr. *J. Am. Chem. Soc.* **2000**, *122*, 12207−12219.
(8) Nordlund, P.; Sjöberg, B.-M.; Eklund, H. *Nature* **1990**, *345*, 593−598.
(9) Nordlund, P.; Eklund, H. *J. Mol. Biol.* **1993**, *232*, 123−164.
(10) Kauppi, B.; Nielsen, B. B.; Ramaswamy, S.; Kjøller-Larson, I.; Thelander, M.; Thelander, L.; Eklund, H. *J. Mol. Biol.* **1996**, *262*, 706−720.
(11) Rosenzweig, A. C.; Frederick, C. A.; Lippard, S. J.; Nordlund, P. *Nature* **1993**, *366*, 537−543.
(12) Rosenzweig, A. C.; Nordlund, P.; Takahara, P. M.; Frederick, C. A.; Lippard, S. J. *Chem. Biol.* **1995**, *2*, 409−418.
(13) Elango, N.; Radhakrishnan, R.; Froland, W. A.; Waller, B. J.; Earhart, C. A.; Lipscomb, J. D.; Ohlendorf, D. H. *Protein Sci.* **1997**, *6*, 556−568.
(14) Lindqvist, Y.; Huang, W.; Schneider, G.; Shanklin, J. *EMBO J.* **1996**, *15*, 4081−4092.
(15) Nordlund, P.; Eklund, H. *Curr. Opin. Struct. Biol.* **1995**, *5*, 758−766.
(16) Summa, C. M.; Lombardi, A.; Lewis, M.; DeGrado, W. F. *Curr. Opin. Struct. Biol.* **1999**, *9*, 500−508.
(17) Atkin, C. L.; Thelander, L.; Reichard, P.; Lang, G. *J. Biol. Chem.* **1973**, *248*, 7464−7472.
(18) Dalton, H. *Adv. Appl. Microbiol.* **1980**, *26*, 71−87.
(19) Nagai, J.; Block, K. *J. Biol. Chem.* **1966**, *241*, 1925−1927.
(20) Wallar, B. J.; Lipscomb, J. D. *Chem. Rev.* **1996**, *96*, 2625−2657.
(21) Solomon, E. I.; Brunold, T. C.; Davis, M. I.; Kemsley, J. N.; Lee, S.-K.; Lehnert, N.; Neese, F.; Skulan, A. J.; Yang, Y.-S.; Zhou, J. *Chem. Rev.* **2000**, *100*, 235−349.
(22) Sjöberg, B.-M.; Reichard, P.; Gräslund, A.; Ehrenberg, A. *J. Biol. Chem.* **1977**, *252*, 536−541.
(23) Ormö, M.; deMaré, F.; Regnström, K.; Åberg, A.; Sahlin, M.; Ling, J.; Loehr, T. M.; Sanders-Loehr, J.; Sjöberg, B.-M. *J. Biol. Chem.* **1992**, *267*, 8711−8714.
(24) Åberg, A.; Ormö, M.; Nordlund, P.; Sjöberg, B.-M. *Biochemistry* **1993**, *32*, 9845−9850.
(25) Ormö, M.; Regnström, K.; Wang, Z.; Que, L., Jr.; Sahlin, M.; Sjöberg, B.-M. *J. Biol. Chem.* **1995**, *270*, 6570−6576.
(26) Logan, D. T.; deMaré, F.; Persson, B. O.; Slaby, A.; Sjöberg, B.-M.; Nordlund, P. *Biochemistry* **1998**, *57*, 10798−10807.
(27) Ling, J.; Sahlin, M.; Sjöberg, B.-M.; Loehr, T. M.; Sanders-Loehr, J. *J. Biol. Chem.* **1994**, *269*, 5595−5601.
(28) Logan, D. T.; Su, X.-D.; Åberg, A.; Regnström, K.; Hajdu, J.; Eklund, H.; Nordlund, P. *Structure* **1996**, *4*, 1053−1064.

for the guiding hypotheses concerning reactivity control by wild-type R2.

Materials and Methods

Preparation of Apo R2-W48F/D84E. The construction of plasmid pR2-W48F/D84E has been reported.[3] Overexpression and purification of apo R2-W48F/D84E protein was performed as previously described.[5] Additional purification steps to obtain protein suitable for crystal growth were performed as previously reported.[29] Protein concentration was determined by A_{280} using the value of 109 mM^{-1} cm^{-1} for ϵ_{280} calculated according to the method of Gill and von Hippel.[5,30]

Spectrophotometry and Stopped-Flow Spectrophotometry. All standard absorption spectra were acquired on a Hewlett-Packard HP8453 spectrophotometer. Stopped-flow measurements were carried out as previously described.[6] The experiment of Figure 1 employed the HP8453 spectrophotometer and Hi-Tech SFA-20 Rapid Mixing Accessory. All other stopped-flow experiments were carried out with the KinTek SF-2001 apparatus housed in the anaerobic chamber.[6] The reactive Fe(II)-R2-W48F/D84E complex was prepared as reported.[5] Specific reaction conditions are given in the appropriate figure legend.

Freeze-Quench Mössbauer Experiments. The apparatus and procedure for preparation of freeze-quenched Mössbauer samples[6,31] and the Mössbauer spectrometer[32] have been described. Specific sample attributes and spectrometer conditions are given in the appropriate figure legend.

Preparation of Samples for Resonance Raman Spectroscopy. $^{16}O_2$ samples were prepared by squirting (with a gas-tight Hamilton syringe) 200 μL of O_2-saturated Fe^{2+} solution (containing 3.1 equiv relative to R2 dimer) into 200 μL of a stirred, O_2-saturated ~2 mM protein solution. The early product sample (brown in color) was incubated for 40 h at 4 °C (to allow the purple complex to form) prior to freezing. The $^{18}O_2$ samples were prepared by initially removing atmospheric oxygen from the protein and iron solutions as previously described.[5] The O_2-free solutions were then evacuated to 25 Torr (as measured by a Cole-Parmer digital manometer) and refilled to ~ 850 Torr with $^{18}O_2$ gas (95% isotopic enrichment; from Icon Services, Mt. Marion, NY). The reaction vessels were sealed and allowed to stir on ice for 1 h prior to mixing (as described above for the $^{16}O_2$ samples). The mixture was incubated for 40 h at 4 °C prior to freezing.

Resonance Raman Spectroscopy. Resonance Raman spectra were obtained with a custom McPherson 2061/207 spectrograph (set to 0.67 m) and a Princeton Instruments (LN-1100PB) liquid-N_2-cooled CCD detector. Rayleigh scattering was attenuated with Kaiser Optical supernotch filters. A krypton laser (Coherent Innova 302) provided excitation at 568 and 647 nm. Relative to the nonresonant vibrational mode of phenylalanine residues at 1004 cm^{-1}, the resonance enhancement of Fe-coordinated phenolate modes was found to be similar at these two excitation wavelengths. Spectra were collected in a 90°-scattering geometry on solution samples at room temperature with a collection time of 20 min. The laser power at the sample was maintained below 50 mW, and the integrity of the Raman samples, before and after laser illumination, was confirmed by direct monitoring of their UV−vis spectra in the Raman capillaries.[33] Frequencies were calibrated relative to indene and CCl_4 standards and are accurate to ±1 cm^{-1}.

Preparation of Crystals of Purple R2-W48F/D84E. Purified apo R2-D84E/W48F was diluted to 10 mg/mL with 100 mM HEPES (pH 7.6) and reacted by addition to the air-saturated protein solution of 6 equiv of Fe(II), which was added from a standardized stock solution of $Fe(NH_4)_2(SO_4)_2 \cdot 6H_2O$ in 5 mN H_2SO_4. The protein solution turned a pale yellow-brown color, and was placed in a refrigerator at ~0 °C. Within 16 h, some protein samples had become purple and were selected for crystallization. After the addition of 1 mM ethyl mercurithiosalicylic acid (EMTS), crystallization was carried out at 37 °C by the hanging drop method. Hanging drops composed of 5 μL of protein solution and 5 μL of precipitant solution were suspended on the lid of a sealed Petri dish containing 5 mL of precipitant solution. The precipitant solution contained 50 mM MES (pH 6.0), 200 mM NaCl, 20% PEG 4000, 0.3% dioxane, and 1 mM EMTS.[34] After equilibration for 7 d, small crystals appeared and were harvested into 750 μL of precipitant solution and homogenized into a suspension of microseeds. The microseed solution was then used in a second round of identical crystallization trials, in which each 10 μL hanging drop was streaked with microseeds by using a cat whisker. Large crystals (0.20 × 0.20 × 0.75 mm^3) suitable for data collection appeared within 2 d of seeding. Crystals were harvested and placed in a cryosolvent consisting of precipitant solution with 20% glycerol. After 3−5 min, the crystals were mounted in rayon loops and immediately frozen in liquid nitrogen. The crystals belong to the space group $P2_12_12_1$ with unit cell dimensions $a = 74.1$, $b = 83.1$, and $c = 114.7$ Å.

Table 1. Data Collection and Refinement Statistics

Data Collection[a]	
resolution range (Å)	30−1.83
no. of total observations	559 295
no. of unique observations	62 044
completeness (%)[b]	97.0 (94.4)
R_{sym}[c]	0.060 (0.240)
Refinement	
resolution range (Å)	30−1.83
no. of reflections	59 536
R-factor[d]	0.204
R-free	0.242
no. of nonhydrogen protein atoms	5568
no. of solvent atoms	316
rms bond length (Å)	0.006
rms bond angles (deg)	1.0
av *B* value (Å^2)	30.47

[a] Data collected at −160 °C using a 2*k* × 2*k* Mar CCD detector at the DND-CAT beamline at the Advanced Photon Source. Wavelength, 1.000 Å. [b] Values in parentheses are for the highest resolution shell: 1.86−1.83 Å. [c] $R_{sym} = \sum|I_{obs} - I_{av}|/\sum I_{obs}$, where the summation is over all reflections. [d] *R*-factor $= \sum|F_{obs} - F_{calc}|/\sum F_{obs}$. Five percent of the reflections were reserved for calculation of *R*-free.

X-ray Diffraction Data Collection and Model Refinement. Diffraction data to 1.83-Å resolution were collected at −160 °C at the Dupont-Northwestern-Dow Collaborative Access Team (DND-CAT) beamline at the Advanced Photon Source using a 2*k* × 2*k* Mar CCD detector, and were processed with the programs DENZO and SCALEPACK (Table 1).[35] The structure was refined with CNS[36] using the refined coordinates of oxidized R2-D84E[29] without solvent molecules as a starting model. The model was first refined as a rigid body, and then further refined by iterative cycles of positional and simulated annealing refinement, individual *B*-factor refinement, and model rebuilding with the program O.[37] Solvent molecules were modeled into peaks $>3\sigma$ in $F_o - F_c$ electron density maps, and were retained if the *B*-values refined to <65 Å^2. The progress of the refinement was monitored by the *R*-free, which was calculated using 5% of the data (Table 1). A Ramachandran plot calculated with PROCHECK[38] shows that 94.1% of the residues in the structure fall in the most favored regions, with 5.9% in the additionally allowed regions. The average error in coordinate positions was estimated to be 0.21 Å by a Luzzati plot, and to be 0.15 Å by σ-weighted calculations. Figure 6A was generated with BOBSCRIPT[39] and Figures 6B and 6C were generated with MOLSCRIPT[40] and RASTER3D,[41] respectively.

(29) Voegtli, W. C.; Khidekel, N.; Baldwin, J.; Ley, B. A.; Bollinger, J. M., Jr.; Rosenzweig, A. C. *J. Am. Chem. Soc.* **2000**, *122*, 3255−3261.
(30) Gill, S. C.; von Hippel, P. H. *Anal. Biochem.* **1989**, *182*, 319−326.
(31) Bollinger, J. M., Jr.; Tong, W. H.; Ravi, N.; Huynh, B. H.; Edmondson, D. E.; Stubbe, J. *Methods Enzymol.* **1995**, *258*, 278−303.
(32) Ravi, N.; Bollinger, J. M., Jr.; Huynh, B. H.; Edmondson, D. E.; Stubbe, J. *J. Am. Chem. Soc.* **1994**, *116*, 8007−8014.
(33) Loehr, T. M.; Sanders-Loehr, J. *Methods Enzymol.* **1993**, *226*, 431−470.
(34) Nordlund, P.; Uhlin, U.; Westergren, C.; Joelson, T.; Sjöberg, B.-M.; Eklund, H. *FEBS Lett.* **1989**, *258*, 251−254.
(35) Otwinowski, Z.; Minor, W. *Methods Enzymol.* **1997**, *276*, 307−326.
(36) Brunger, A. T.; Adams, P. D.; Clore, G. M.; DeLano, W. L.; Gros, P.; Grosse-Kunstleve, R. W.; Jiang, J.-S.; Kuszewski, J.; Nilges, M.; Pannu, N. S.; Read, R. J.; Rice, L. M.; Simonson, T.; Warren, G. L. *Acta Crystallogr.* **1998**, *D54*, 906−921.
(37) Jones, T. A.; Zou, J.-Y.; Cowan, S. W.; Kjeldgaard, M. *Acta Crystallogr.* **1991**, *A47*, 110−119.
(38) Laskowski, R. A. *J. Appl. Crystallogr.* **1993**, *26*, 283−291.

Gas Chromatographic/Mass Spectral (GC/MS) Analysis for ϵ-Hydroxyphenylalanine Production in R2-W48F/D84E and Other R2 Variants. Protein samples (0.5 mg) for mass spectroscopy were precipitated with 0.2 volumes of 50% (w/v) aqueous trichloroacetic acid, and the pellet was washed with 500 μL of distilled deionized water. The protein precipitate was resuspended in 200 μL of 6 N HCl and incubated under nitrogen for 24 h at 100 °C. The hydrolyzed samples were dried by evaporation on a Speed-Vac concentrator (Savant Instruments). The lyophilized products were converted to *tert*-butyldimethylsilyl derivatives by addition of 100 μL of (*N*-methyl-*N*-*tert*-butyldimethylsilyl)trifluoroacetamide (Regis Technologies, Inc., Morton Grove, IL) followed by incubation at 60 °C for 1 h. Aliquots of 1.0 μL were analyzed by GC/MS using a model 5890 Series II gas chromatograph coupled to a model 5972 mass spectrometer (Hewlett-Packard, Palo Alto, CA) using 70 eV electron ionization. Splitless injection was made onto a 30 m DB-1 column (J&W Scientific, Folsom, CA) with 0.25 mm inner diameter and 0.25 μm film with the injector held at 250 °C. Helium was used as carrier gas at a linear velocity of 35 cm/s, and the column temperature was programmed from 80 °C (4 min hold) to 285 °C at 8 deg/min, with a final 10 min hold at 285 °C. Selected ion monitoring of *m*/*z* 466 and 302 was performed with a dwell time of 100 ms for each channel. Retention times were determined for standards of tyrosine and δ- and ϵ-hydroxyphenylalanine (Sigma Chemical Co., St. Louis, MO), and quantitative analyses were performed based on experimental relative response factors for peak areas for *m*/*z* 466, which corresponds to the abundant [M − *tert*-butyl]$^+$ peak for each isomer.

Reduction of the Peroxo Intermediate/Interception of the Hydroxylating Intermediate by Dithionite. Reactant solutions were mixed (as described in the legend to Figure 9) with an Update Instruments System 1000 Ram Drive.[6] Samples of ~500 μL were prepared. Dithionite was rapidly removed by gel filtration on a 2 mL Sephadex G-25 "spin column" centrifuged at 1500 × g for 2 min. The samples were then incubated for 35 h at 4 °C prior to acquisition of their absorption spectra.

X-ray Absorption Spectroscopy. X-ray absorption spectra of four brown and four purple samples were acquired on beamline 7-3 at SSRL (3.0 GeV, 100 mA) using a Canberra 13 element Ge solid-state detector to monitor Fe Kα fluorescence and an Oxford continuous flow liquid Helium cryostat to maintain sample temperature at 10 K. Equal volumes of O_2-saturated solutions of Fe(II) (in 5 mN H_2SO_4) and apo R2-W48F/D84E (Fe(II)/R2 = 3.1) were mixed at 5 °C, and the solutions were allowed to react on ice for <30 min (brown) or for 40 h (purple) prior to freezing for transport. Samples were thawed briefly to load into a Lucite EXAFS cell with a polypropylene window. Alternatively, samples were quenched at the appropriate reaction time into liquid isopentane at −140 °C and packed into a dual Mössbauer/EXAFS sample cup.[42] On the basis of the molar absorptivity ($\epsilon_{550\ nm}$) of the purple complex reported below, between 18 and 32% of the Fe in the EXAFS samples underwent the brown-to-purple transition.

k^3 weighted EXAFS spectra were Fourier transformed over a range from 1 to 13 or 14 Å^{-1}. The first shell was simplified for fitting by back-transformation. Quality of fit was judged by two parameters, *F* and ϵ'; the latter corrects the goodness of fit, *F*, for the number of variable parameters used. Both are defined elsewhere.[42,43] The absorber−scatterer distance, *R*, and the root-mean-squared deviation in bond length, σ, were varied for each shell. The remaining details of the data collection and reduction were as previously described.[42,43]

Results

Characterization of O_2 Activation in R2-W48F/D84E by Stopped-Flow Absorption and Freeze-Quench Mössbauer Methods. Mixing of apo R2-W48F/D84E with Fe(II) in the presence of O_2 (Figure 1) or of the preformed Fe(II)-R2-W48F/D84E complex with O_2-saturated buffer (not shown) leads to development of the intense 700-nm absorption characteristic of the μ-1,2-peroxodiiron(III) intermediate. Under the conditions employed in the experiment of Figure 1 (see legend), this feature develops and decays with apparent first-order rate constants of 2.3 ± 0.3 and 0.26 ± 0.03 s^{-1}, respectively. Component analysis of the Mössbauer spectra (Figure 2) of a series of freeze-quenched samples prepared under identical reaction conditions demonstrates that, as expected, the 700-nm feature is temporally correlated (Figure 3) with the Mössbauer quadrupole doublet features that were previously ascribed to the peroxo intermediate.[2] The fraction of the total iron absorption contributed by these features reaches a maximum of 57 ± 3% (in Figure 2, spectrum B), which corresponds to 1.8 ± 0.2 equiv of Fe or 0.9 ± 0.1 equiv of peroxodiiron(III) complex (the Fe/R2 ratio was 3.1 ± 0.1 in this experiment). Because the rate constant for decay of the intermediate (0.26 s^{-1}) is not negligible with respect to the rate constant for its formation (2.3 s^{-1}), <1 equiv is expected to accumulate per equivalent of reactant. In fact, from kinetic simulations it can be determined that accumulation of 0.9 equiv of an intermediate that forms and decays with these rate constants requires ~1.2 equiv of reactant, implying that 2.4 ± 0.3 equiv of Fe(II) reacts through the pathway in which the peroxodiiron(III) complex is an intermediate. Given that the dimeric apo protein can incorporate 2.5−3.0 equiv of added Fe(II),[44] it is clear that this mechanistic pathway is the predominant one. The data of Figure 3 permit the molar absorptivity at 700 nm of the peroxo intermediate to be estimated as 1800 ± 300 M^{-1} cm^{-1}.[45]

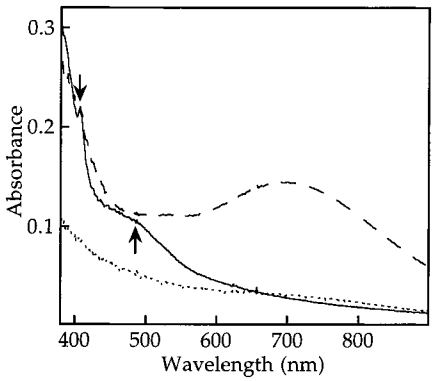

Figure 1. O_2 activation by R2-W48F/D84E monitored by stopped-flow spectrophotometry. Development of the absorption spectrum was monitored after equal-volume mixing at 5 °C of O_2-saturated solutions of 0.14 mM apo protein in 100 mM Na-Hepes (pH 7.6) and 0.41 mM $FeSO_4$ in 5 mN H_2SO_4. The spectra shown were acquired immediately after mixing (dotted trace; estimated deadtime is 0.1 s), 1.1 s after mixing (dashed trace), and 20 s after mixing (solid trace).

Decay of the peroxo species is associated with the formation of a mixture of products. The absorption spectrum after decay of the intermediate (Figure 1, solid trace) exhibits the sharp 409-nm feature of the Y122• (marked by the downward arrow), but the height of this peak and the value of $\epsilon_{409} - (\epsilon_{403} + \epsilon_{415})/2$

(39) Esnouf, R. M. *J. Mol. Graphics & Modell.* **1997**, *15*, 132−134.
(40) Kraulis, P. J. *J. Appl. Crystallogr.* **1991**, *24*, 946−950.
(41) Merritt, E. A.; Bacon, D. J. *Methods Enzymol.* **1997**, *277*, 505−524.
(42) Riggs-Gelasco, P. J.; Shu, L.; Chen, S.; Burdi, D.; Huynh, B. H.; Que, L., Jr.; Stubbe, J. *J. Am. Chem. Soc.* **1998**, *120*, 849−860.
(43) Riggs-Gelasco, P. J.; Mei, R.; Yocum, C. F.; Penner-Hahn, J. E. *J. Am. Chem. Soc.* **1996**, *118*, 2387−2399.

(44) The reason that the protein takes up less than its theoretical complement of 4 Fe per dimeric subunit is not clear, but very similar (less-than-theoretical) stoichiometries have been determined for the wild-type protein and all other variants prepared by our group and others.

(45) Preliminary results with a related R2 variant (W48A/D84E) indicate that the peroxo complex accumulates to an even greater extent during O_2 activation by this protein. The current best estimate of ϵ_{700} of the complex from these results is 2100 M^{-1} cm^{-1}. It is not yet clear whether the difference from the value calculated from the R2-W48F/D84E data reflects experimental uncertainty or real variation in ϵ_{700} from one R2 variant to another.

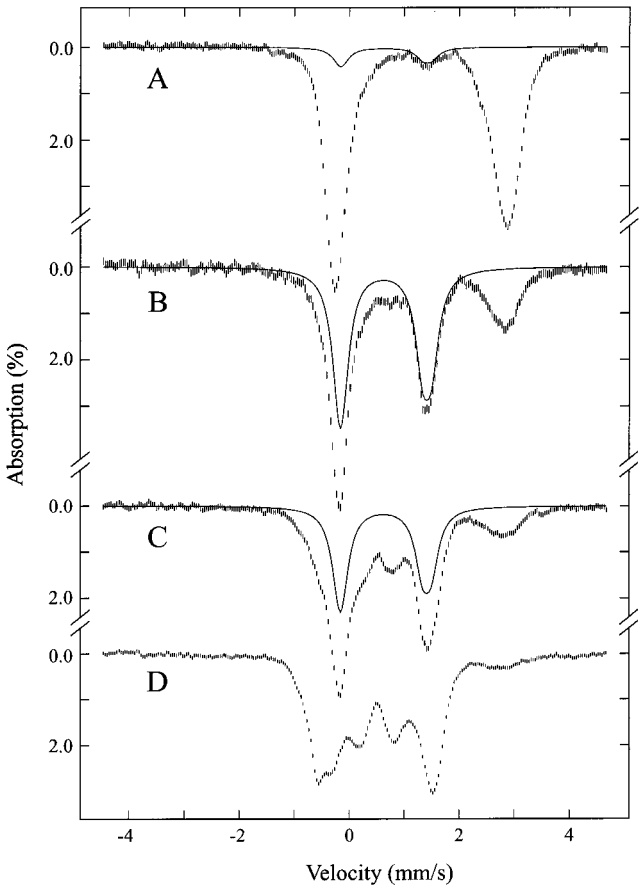

Figure 2. Mössbauer spectra of freeze-quenched samples from the reaction of 0.56 mM apo R2-W48F/D84E, 1.7 mM Fe(II), and 1.9 mM O_2 at 5 °C in 50 mM Na-Hepes (pH 7.6). The samples were quenched at reaction times of 0.025 (A), 0.80 (B), 3.0 (C), and 60 s (D). The spectra were acquired at 4.2 K with a magnetic field of 50 mT applied parallel to the γ-beam. In spectra A−C, the solid trace plotted over each experimental spectrum is a theoretical spectrum of the peroxo intermediate (two doublets with $\delta(1) = 0.60$ mm/s, $\Delta E_Q(1) = 1.48$ mm/s and $\delta(2) = 0.66$ mm/s, $\Delta E_Q(2) = 1.67$ mm/s) plotted at the appropriate fraction of the total iron absorption. The features of the intermediate overlap with those of a major product. Consequently, the peroxo spectrum appears to underestimate the area attributable to the intermediate in the later spectra when more of the overlapping product has formed. Detailed component analysis of all the spectra from the timecourse determines the percentages of the peroxo intermediate.

(which we determined as previously described[46] to be 2150 ± 50 $M^{-1}cm^{-1}$) indicate that only ~0.17 equiv Y122• is produced under these conditions.[47] The features characteristic of the normal μ-oxodiiron(III) cluster (shoulder at 325 nm and broad peak at 365 nm) are also less prominent than those for the products of either the wt R2 reaction or the R2-D84E reaction.[2,46] These observations indicate that altered products predominate in the R2-W48F/D84E reaction. A shoulder at ~490 nm (upward arrow in Figure 1), which is absent in the spectra of product samples from the reactions of other R2 variants (including the wt protein), is apparent in the spectra of the R2-W48F/D84E early product samples. Along with other absorption features, this shoulder contributes to the brown tint of the early product samples. Logan et al. ascribed a similar feature in the

(46) Bollinger, J. M., Jr.; Tong, W. H.; Ravi, N.; Huynh, B. H.; Edmondson, D. E.; Stubbe, J. *J. Am. Chem. Soc.* **1994**, *116*, 8015−8023.

(47) Somewhat greater quantities of Y122• can be obtained under different reaction conditions. For example, a lower ratio of Fe(II)/R2 favors formation of more radical, leading to as much as ~0.25 equiv. We do not yet understand this behavior.

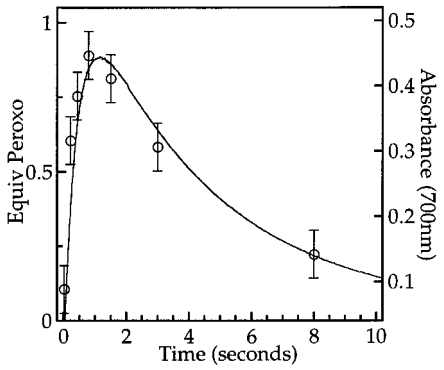

Figure 3. Kinetics of formation and decay of the peroxo intermediate as deduced by component analysis of the Mössbauer spectra (circular points, left axis) compared to the kinetics of absorbance at 700 nm (solid trace, right axis). The reaction conditions are given in the legend to Figure 2. The path length on the KinTek stopped-flow apparatus used to acquire the absorbance data is 0.5 cm.

spectra of the products of O_2 activation by R2-Y122F/E238A to a complex resulting from coordination of the F208-derived, neutral phenol to Fe2 of the cluster.[26] Given that F208 is also hydroxylated in the R2-W48F/D84E reaction, the assignment of Logan et al. is possibly applicable here as well.

The Mössbauer spectrum of the early (brown) product of the R2-W48F/D84E reaction (Figure 2, spectrum D) corroborates the conclusion that altered diiron products predominate. The spectrum reflects the presence of both diamagnetic and paramagnetic species. The paramagnetic features contribute 33 ± 3% of the total absorption area attributable to iron (Figure S1A, Supporting Information). The diamagnetic portion of the spectrum is complex. For this reason, its deconvolution into component subspectra is subject to some uncertainty. Nevertheless, the diamagnetic region can be decomposed into five quadrupole doublets having isomer shift (δ) and quadrupole splitting (ΔE_Q) parameters that are characteristic of high-spin Fe(III) complexes (Figure S1B and Table S1, Supporting Information), and by summation of these doublets together with the spectra of the Fe(II) reactant and the peroxodiiron(III) intermediate (each with an appropriate weighting factor), all spectra from a complete reaction timecourse can be satisfactorily reproduced. The multiplicity of Fe(III) products in the R2-W48F/D84E reaction contrasts with the outcome of the wild-type R2 reaction, in which the μ-oxodiiron(III) cluster is produced almost exclusively.

Slow Conversion of the Early Product to a Purple Complex. Upon prolonged (many hours) incubation at 0 °C, the brown early product samples become intensely purple due to the development of a broad absorption band centered at ~550 nm (Figure 4). This feature develops with a rate constant of 0.10 ± 0.02 h^{-1} (inset to Figure 4). The final absorbance at 550 nm was observed to vary significantly (from 1.0 to 2.1 mM^{-1} cm^{-1} on the basis of protein concentration), even for samples prepared by very similar reaction protocols. Less absorption develops when incubation of the brown product is carried out at higher temperatures, and in this case, subsequent incubation at 0 °C does not result in development of additional absorption. These observations suggest that alternative pathways (other than that leading to the purple product) for decay of the brown precursor become accessible at higher temperatures and that these pathways are not reversible.

Characterization of the Purple Product by Resonance Raman (RR) Spectroscopy. The expectation that R2-W48F/D84E would mediate a two-electron oxidation reaction, the

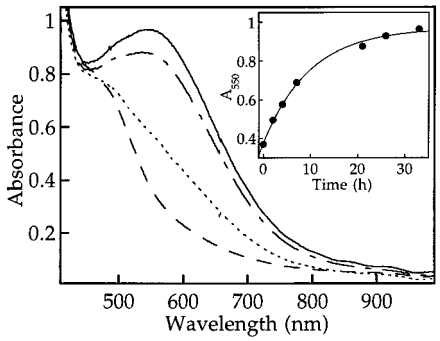

Figure 4. Changes in the absorption spectrum of R2-W48F/D84E associated with conversion of the initial brown product to the purple product. The initial product sample was prepared by equal-volume hand mixing at ~5 °C of O_2-saturated 1.5 mM apo R2-W48F/D84E (in 100 mM Na-Hepes, pH 7.6) with O_2-saturated 4.5 mM $FeSO_4$ (in 5 mN H_2SO_4). The spectra were acquired 1 min (dashed trace), 4 h (dotted trace), 21 h (dot−dashed trace), and 33 h (solid trace) after the solutions were mixed. The inset shows a plot of absorbance at 550 nm as a function of time. The solid trace is a fit of the equation for a first-order growth to the data points. It corresponds to a rate constant of 0.10 h^{-1}.

seminal studies of Sjöberg, Nordlund, and co-workers marking F208 as a potential target,[23,24,28] and the knowledge that (inorganic and protein) Fe(III)−phenolate complexes exhibit absorption features in the 550-nm region (due to phenolate-to-Fe(III) charge-transfer transitions)[48] led us to suspect that the purple product might be a complex between an Fe(III) ion of the cluster and a phenolate derived from hydroxylation of F208. Indeed, excitation within the 550-nm absorption band leads to the appearance of a manifold of vibrational frequencies (Figure 5, spectra A and B), from which the nonresonant Raman signals of the protein matrix may be removed by subtraction of the spectrum of the apo protein (spectrum C) to leave the series of bands at ~600, 1300, 1500, and 1600 cm^{-1} (spectra D and E) that constitute the signature of metal-coordinated phenolates.[48] These difference spectra not only establish the presence of a phenolate−metal ion (presumably Fe(III)) complex in purple R2-W48F/D84E but also rule out the possibility that this complex results from coordination of a preexisting tyrosine residue. The ν(C═C) phenolate modes at 1484 and 1580 cm^{-1} (Figure 5, spectra D and E) are ~20 cm^{-1} downshifted from the frequencies of iron−tyrosinate chromophores found in several other proteins.[48−52] These frequency shifts may be rationalized (as confirmed by the crystallographic data presented below) by the meta-substitution of the F208-derived phenolate as opposed to the para-substitution of normal tyrosine. More definitively, in samples for which the reaction was carried out in the presence of $^{18}O_2$, multiple shifts are observed in the RR difference spectra (Figure 5, spectrum E vs spectrum D). The bands at 1281 and 615 cm^{-1} show the largest ^{18}O-downshifts (8 and 18 cm^{-1}, respectively) owing to their significant ν(C−O) and ν(Fe−O) character, respectively. The 1273 and 597 cm^{-1} bands of the product prepared with $^{18}O_2$ show at most weak "shoulders" from the corresponding bands of the ^{16}O-containing

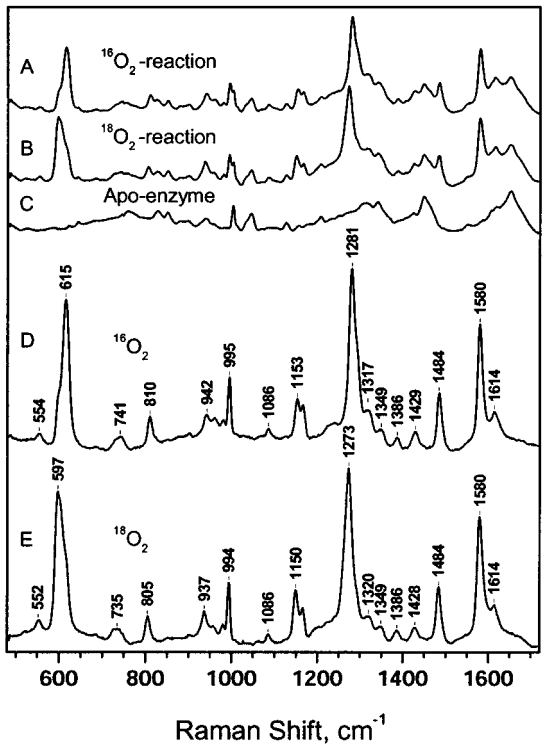

Figure 5. Resonance Raman spectra of purple R2-W48F/D84E obtained with 647-nm excitation. Samples were prepared (as described in Materials and Methods) by reaction of the apo protein with Fe(II) in the presence of $^{16}O_2$ (trace A) or $^{18}O_2$ (trace B). Traces D and E are the difference spectra obtained by subtraction of the spectrum of the apo protein (trace C) from spectra A and B, respectively.

product. From a simple line shape analysis of these features, an upper limit of 30% can be set for the contribution of ^{16}O-containing product to the spectra of the sample prepared with ^{18}O. Given that the bands in question are associated with coupled vibrational modes, the actual contribution from ^{16}O-containing product is likely to be much smaller than this. Thus, the O-atom in the Fe−phenolate complex in purple R2-W48F/D84E originates from molecular oxygen and loss of the ^{18}O label to solvent ("wash-out") occurs to a minor extent, if at all. These RR data demonstrate that the protein effects a self-hydroxylation reaction by an oxygen-atom-transfer mechanism.

Structural Characterization of the Purple Product by X-ray Crystallography. More detailed structural insight, including the identity of the aromatic side chain that is hydroxylated, was sought by X-ray crystallography. Diffraction data for two particularly purple crystals were used for two independent structure determinations (as described in Materials and Methods). The better of these yielded a 1.83-Å resolution structure, which is discussed below and summarized in Tables 1 and 2. No qualitative structural differences were observed in the second independent determination. After the initial refinement cycle, a strong peak in the $F_o - F_c$ difference electron density map was observed between Fe2 and the ϵ-carbon of F208 (Figure 6A) at a location appropriate for an oxygen atom bonded to both. When considered with the absorption (Figure 4) and resonance Raman data (Figure 5) and the aforementioned precedent,[26] this observation indicates that F208 has undergone hydroxylation at the ϵ-carbon and the inserted oxygen has become coordinated by Fe2. Residue 208 was therefore assigned as ϵ-hydroxyphenylalanine in subsequent refinement cycles. Occupancy refinement and inspection of difference Fourier maps indicate that all residues ligating the diiron cluster and all iron ions are >95% occupied in both subunits. There is no evidence

(48) Que, L., Jr. In *Iron Carriers and Iron Proteins*; Loehr, T. M., Ed.; VCH Publishers: New York, 1989; pp 467−524.
(49) Que, L., Jr.; Heistand, R. H., II; Mayer, R.; Roe, A. L. *Biochemistry* **1980**, *19*, 2588−2593.
(50) Averill, B. A.; Davis, J. C.; Burman, S.; Zirino, T.; Sanders-Loehr, J.; Loehr, T. M.; Sage, J. T.; Debrunner, P. G. *J. Am. Chem. Soc.* **1987**, *109*, 3760−3767.
(51) Siu, D. C.; Orville, A. M.; Lipscomb, J. D.; Ohlendorf, D. H.; Que, L., Jr. *Biochemistry* **1992**, *31*, 10443−10448.
(52) Waldo, G. S.; Ling, J.; Sanders-Loehr, J.; Theil, E. C. *Science* **1993**, *259*, 796−798.

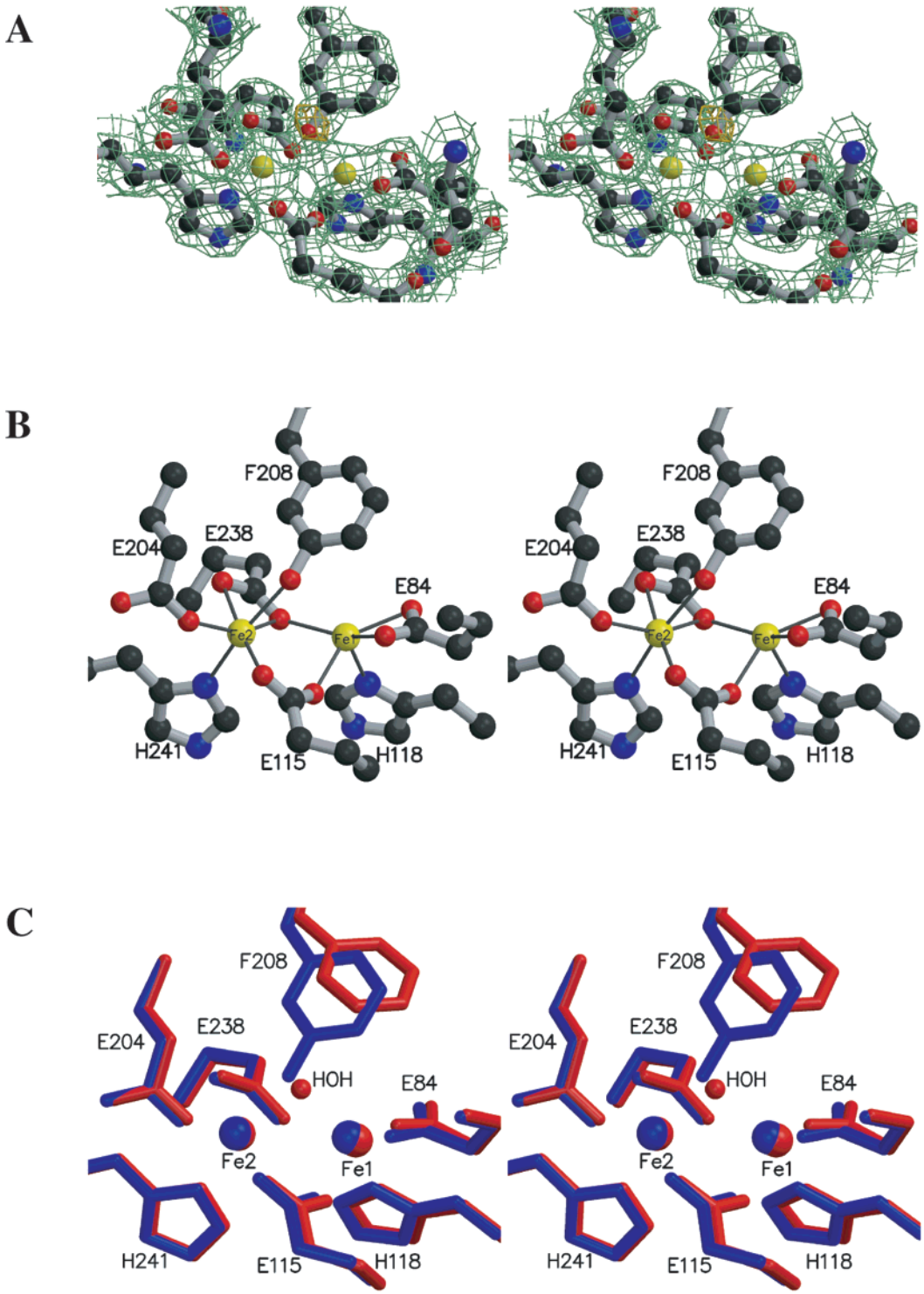

Figure 6. Crystal structure of the purple product in R2-W48F/D84E. (A) Stereoview of the final 1.83-Å resolution $2F_o - F_c$ electron density map at the diiron center (green, contoured at 1.1σ). The $F_o - F_c$ difference electron density map showing the hydroxylation of F208 at the ϵ carbon is superimposed (gold, contoured at 3σ). The iron ions are in yellow. The orientation is the same as in parts B and C. (B) Stereoview of the diiron center. The two active sites in the dimer exhibit the same coordination geometry. (C) Stereosuperposition of the diiron centers in the R2-D84E/W48F purple product (blue) and in reduced R2-D84E (red).

for structural heterogeneity in the electron density maps. In the refined structure, the hydroxylated ϵ-carbon is shifted 1.6 Å relative to its position in oxidized R2-D84E (Figure 6C),[29] allowing the inserted O-atom to coordinate to Fe2 with an average Fe−O bond distance of 2.38 Å. The phenolate oxygen occupies essentially the same site as a bound H_2O molecule in the structure of reduced R2-D84E[29] and N_3^- in the structure of the azide complex of R2-Y122F/F208A.[53] The displacement of the phenyl ring relative to its position in R2-D84E is achieved by a 0.9 Å shift at the C_γ position combined with a 30° ring plane rotation toward Fe2 about the C_β−C_γ bond. The ϵ-hy-

(53) Andersson, M. E.; Högbom, M.; Rinaldo-Matthis, A.; Andersson, K. K.; Sjöberg, B.-M.; Nordlund, P. *J. Am. Chem. Soc.* **1999**, *121*, 2346−2352.

Table 2. Interatomic Distances (Å) in "Purple" R2-D84E/W48F.

atom	atom	monomer A	monomer B	av
Fe1	Fe2	3.43	3.40	3.42
Fe1	Glu84 Oϵ1	2.25	2.24	2.25
	Glu84 Oϵ2	2.41	2.39	2.40
	Glu115 Oϵ1	2.21	2.26	2.24
	His118 Nδ1	2.20	2.25	2.23
	Glu238 Oϵ1	2.27	2.40	2.34
Fe2	Glu115 Oϵ2	2.27	2.09	2.18
	Glu204 Oϵ1	2.23	2.29	2.26
	Glu238 Oϵ1	2.31	2.38	2.35
	Glu238 Oϵ2	2.22	2.29	2.26
	His241 Nδ1	2.31	2.29	2.30
	Phe208 *m*O	2.30	2.45	2.38

droxyphenylalanine thus occupies a position similar to that of the same ligand in the self-hydroxylating R2-Y122F/E238A protein,[26] though the Fe−$O_{phenolate}$ distance is significantly shorter in R2-W48F/D84E. This short distance implies that the phenolic O-atom is deprotonated.

The geometry of the diiron center (Figure 6B) is very similar to that observed in the structure of reduced R2-D84E.[29] The average Fe−Fe distance is 3.42 Å (compared to the 3.5 Å determined for reduced R2-D84E), and there is no evidence in the electron density maps for an oxo bridge (Figure 6A). The two irons are bridged by E238 in a μ-(η^1,η^2) mode, and E84 is bidentate to Fe1. E204 adopts an anti-monodentate, terminal coordination mode like that observed in R2-D84E. Fe1 is five coordinate and Fe2 is six coordinate. The fact that the cluster more closely resembles that in *reduced* R2-D84E than that in *oxidized* R2-D84E might be taken as evidence that the R2-W48F/D84E purple product is in the II,II or II,III oxidation state. However, the Mössbauer and X-ray absorption data clearly indicate that all the Fe in the purple sample is in the III oxidation state (vide infra). It appears that the coordination of the phenolate ligand is sufficient to cause a coincidental structural similarity of this diiron(III) product to the diiron(II) form of R2-D84E.

In reduced wt R2, a hydrogen bond links the uncoordinated side chain oxygen atom of D84 to the phenolic hydroxy group of Y122.[28] In reduced R2-D84E, this hydrogen bond is broken due to a 1 Å shift of the phenolic hydroxy group of Y122 away from Fe1 and to the bidentate coordination mode of E84.[29] The distance from the closest oxygen atom of E84 to the phenolic hydroxy group of Y122 is 4.50 Å. In "purple" R2-D84E/W48F, the positions of both E84 and Y122 are nearly identical with those in reduced R2-D84E. However, an additional water molecule, not observed in reduced R2-D84E, is hydrogen bonded to both E84 and the phenolic hydroxy group of Y122. Although replacement of W48 with a phenylalanine residue removes a hydrogen bond between residue 48 and D237, the remainder of this hydrogen bonding network, connecting D237 to iron ligand H118, remains intact.

Timing and Yield of the Hydroxylation Reaction. The remarkably slow formation of the purple Fe(III)−phenolate product raises the question of whether F208 hydroxylation results directly from the primary O_2 activation pathway (through the peroxo intermediate) or from some slow, "adventitious" (i.e., uninteresting) side reaction. Two lines of chemical evidence unequivocally establish that the hydroxylation takes place during the decay of the peroxo intermediate and *not* during the very slow transition to the purple species. In the first, ϵ-hydroxyphenylalanine was quantified in both brown and purple samples by total hydrolysis of the protein and GC/MS analysis of the *tert*-butyldimethylsilyl derivatives of the free amino acids. Apo R2-W48F/D84E was mixed in the presence of O_2 with Fe(II), and the reaction was allowed to proceed at 5 ± 2 °C for approximately 60 s. A portion of the brown product was "quenched" as described in the Methods section by addition of trichloroacetic acid. The remainder of the sample was incubated on ice for 48 h to allow for conversion to the purple complex prior to precipitation of the protein with trichloroacetic acid. Following acid hydrolysis and derivatization, identical quantities of ϵ-hydroxyphenylalanine derivative (0.35 equiv) were found in the brown and purple R2-W48F/D84E samples, whereas less than 0.004 equiv was detected in analysis of unreacted apo R2-W48F/D84E. The identical analysis applied to the apo and Fe(II)/O_2-reacted forms of wt R2, R2-W48F, and R2-D84E in all cases revealed less than 0.012 equiv of ϵ-hydroxyphenylalanine derivative (less than 4% of the *minimum* quantity detected in reacted R2-W48F/D84E). These results demonstrate that the initial brown product has already undergone hydroxylation of F208 and that both substitutions (W48F and D84E) are required for this outcome.

With the absorption spectrum of the purple product taken prior to its preparation for GC/MS analysis and the quantity of ϵ-hydroxyphenylalanine determined by this analysis, the molar absorptivity of the Fe(III)−phenolate species can be calculated (ϵ_{550} = 4200 ± 600 M^{-1} cm^{-1}). An assumption of this calculation is that all of the ϵ-hydroxyphenylalanine becomes part of the Fe(III)−phenolate complex. By using this value of ϵ_{550}, it may be calculated that the highest yield of ϵ-hydroxyphenylalanine among all samples was 0.5 equiv. This is less than the 1.25−1.5 equiv that could theoretically form from the 2.5−3.0 equiv of Fe(II) that the apo protein can incorporate. Thus, F208 hydroxylation is a major product, but not the exclusive product, of O_2 activation in R2-W48F/D84E. The substoichiometric yield of ϵ-hydroxyphenylalanine seems incompatible with the homogeneity of the crystalline purple product indicated by the X-ray diffraction data. This apparent discrepancy may be rationalized quite simply (albeit tentatively) by the proposal that the Fe(III)−phenolate-containing product *crystallizes selectively* due to enhanced stability or differences in surface characteristics with respect to the other species present in the heterogeneous product solution.[54]

The conclusion that F208 hydroxylation occurs during formation of the initial brown product and not during the slow conversion to the purple product is corroborated by results of experiments in which the hydroxylating intermediate was intercepted with the strong and facile one-electron reductant, dithionite. Sequential-mixing stopped-flow experiments revealed that decay of the peroxo intermediate is accelerated by dithionite (Figure 7). The observed rate constant for decay "saturates" with increasing [dithionite] at a value of 1.0 ± 0.1 s^{-1} (inset to Figure 7). This modest and saturable acceleration suggests that the peroxo complex is relatively (or perhaps completely) unreactive toward reduction by dithionite and that a unimolecular step (e.g., conversion to a more reactive diiron complex or a protein conformational change) rate-limits reduction at high dithionite concentrations. By the following Mössbauer experiment, it was verified that the products resulting from decay of the intermediate in the presence of "saturating" dithionite contain Fe(III) rather than Fe(II). For one sample (Figure 8, spectrum A) the peroxo intermediate was allowed to reach its maximum con-

(54) There is anecdotal evidence that this sort of selective crystallization occurs for the wild-type R2 protein. For example, an Fe per R2 stoichiometry of 2.8−3.2 has been reported by three different groups, who purified the protein by three distinct procedures. Nevertheless, when the protein has been subjected to crystallographic analysis, full occupancy of the iron sites has invariably been observed.

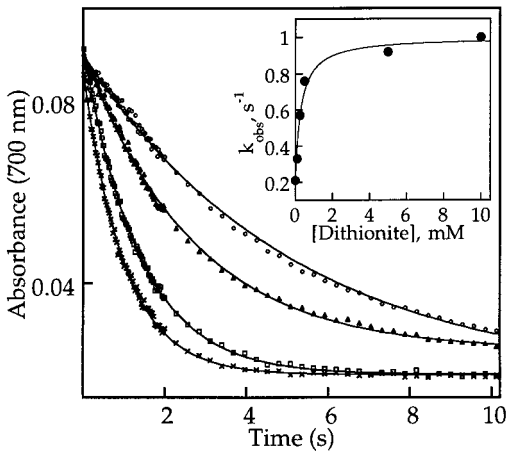

Figure 7. Acceleration of decay of the 700-nm absorption of the peroxo complex by dithionite. An air-saturated solution of 0.36 mM apo R2-W48F/D84E (in 100 mM Na-Hepes, pH 7.6) was first mixed at 5 °C with an equal volume of an air-saturated solution of 1.3 mM Fe-$(NH_4SO_4)_2$ (in 5 mN H_2SO_4), the reaction was allowed to proceed for 1.35 s, and the reaction solution was then mixed with 0.5 equivalent volume of sodium dithionite (varying concentration in O_2-free 100 mM Na-Hepes, pH 7.6) immediately prior to acquisition of data. The dithionite concentrations after mixing were 0 (circular points), 0.1 (triangular points), 0.5 (square points), and 10 mM (× points). The solid traces are fits of the equation for a first-order decay to the data. The inset shows the rate constants obtained from these fits plotted versus dithionite concentration. The solid trace in the inset is a fit of the equation for a hyperbola to the data.

centration (at 0.9 s) and the sample was then freeze-quenched to trap the intermediate for quantitation. Analysis of its spectrum indicates that 0.9 ± 0.1 equiv of peroxo species was trapped in this sample along with 1.3 ± 0.2 equiv of unreacted Fe(II) (solid line plotted over data). For a second sample (Figure 8, spectrum B), the intermediate was allowed to accumulate for 0.9 s prior to mixing with dithionite (final concentration of 10 mM). Decay of the intermediate was allowed to proceed to completion (∼ 20 s) before the sample was frozen for analysis. The Mössbauer spectrum of this sample shows that no additional Fe(II) ion is generated upon decay of the peroxo complex in the presence of dithionite. Thus, dithionite accelerates conversion of the peroxo complex to Fe(III) products. The simplest interpretation is that the intermediate satisfies one or both of its oxidizing equivalents by reaction with the strong, exogenous reductant. Decay of the complex under these conditions *should not*, therefore, lead to hydroxylation of F208Y, which is a *two-electron* oxidation. Indeed, the presence of dithionite during decay of the intermediate prevents development of the 550-nm absorption of the Fe(III)−phenolate product upon subsequent removal of the reductant and incubation at 0 °C (Figure 9, dashed trace). By contrast, addition of dithionite immediately after decay of the peroxo complex (at a reaction time of 2 min) *does not* reduce the quantity of the Fe(III)−phenolate product that develops upon subsequent removal of the reductant and incubation at 0 °C (Figure 9, dotted trace). Thus, dithionite can apparently prevent the hydroxylation outcome, presumably by enforcing sequential one-electron reduction of the hydroxylating intermediate, but can do so only when present *during decay of the peroxo complex*. Together with the GC/MS quantitation of ϵ-hydroxyphenylalanine in the brown and purple species, these observations establish that F208 hydroxylation takes place during decay of the very relevant peroxo intermediate and not during the slow conversion of the brown species to the purple species.

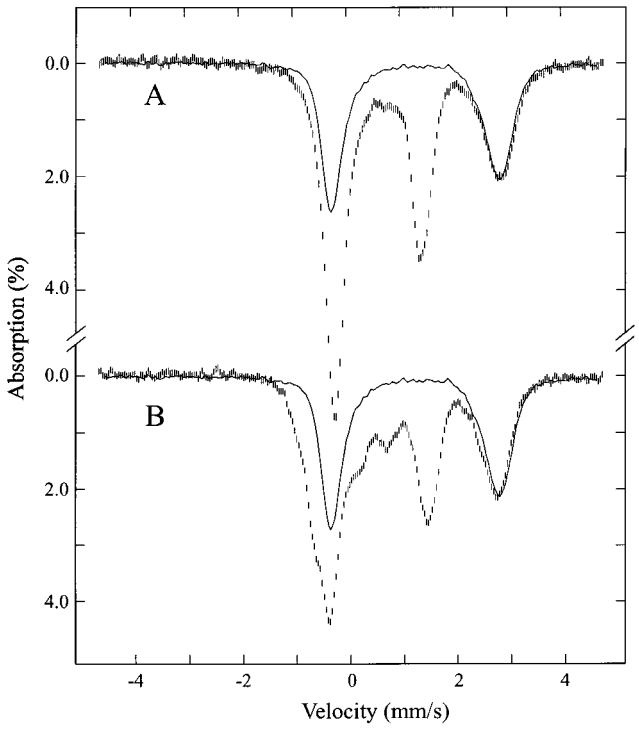

Figure 8. Mössbauer spectra of a 0.9-s freeze-quenched sample (A) and a "dithionite-quenched" sample (B) from the reaction at 5 °C of apo R2-W48F/D84E with Fe(II) and O_2. In preparation of the sample for spectrum A, equal volumes of O_2-saturated solutions of 1.45 mM apo R2-W48F/D84E (in 100 mM Na-Hepes, pH 7.6) and 4.9 mM Fe-$(NH_4SO_4)_2$ (in 5 mN H_2SO_4) were mixed, and the reaction was freeze-quenched after 0.9 s. In preparation of the sample for spectrum B, the first mix was as for spectrum A, but after the 0.9-s aging period the reaction mixture was subsequently mixed with 0.5 equivalent volume of 30 mM sodium dithionite (in O_2-free 100 mM Na-Hepes, pH 7.6). This solution was allowed to age for 20 s before being frozen by manual immersion in liquid N_2. The solid line in each case is the experimental reference spectrum for unreacted Fe(II) plotted at 42% for spectrum A and 43% for spectrum B of the total iron absorption area. This spectrum was generated from the spectrum of the 0.025-s sample in Figure 2 (spectrum A) by subtraction of the small contribution (7%) of the peroxo intermediate.

Nature of the Slow Conversion to the Purple Product. The demonstration that F208 hydroxylation has already occurred in the initial brown product raises the question of what chemical steps the very slow conversion to the purple Fe(III)−phenolate species comprises. Combined Mössbauer and EXAFS data on the brown and purple species strongly suggest that the conversion involves a ligand rearrangement in which a bridging oxygen (most likely a μ-oxo) is lost. Formation of the purple product is associated with the disappearance of Mössbauer quadrupole doublets and the development of paramagnetic features (Figure 10). Subtraction of the experimental spectrum of the purple species (spectrum B) from that of the brown species (spectrum A) removes the contributions of components that do not undergo change in this conversion and resolves the features of only those species that form (spectrum C, downward features) or decay (upward features). (Note that, because spectrum C is a subtraction result, the experimental uncertainty in each data point is twice that for the experimental spectra.) The features that are lost can be simulated with three quadrupole doublets. The vast majority of the lost intensity (28%) comprises two equally intense doublets having quadrupole splittings of 1.72 and 2.15 mm/s. In addition, a small fraction (corresponding to 3% of the total iron absorption) of the component having $\Delta E_Q = 0.57$

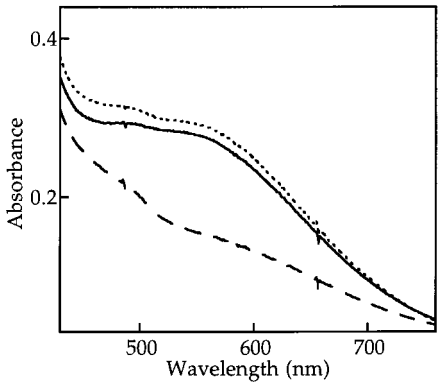

Figure 9. Suppression of subsequent development of the purple complex upon reduction of the peroxo intermediate by dithionite. Equal volumes of O_2-saturated solutions of 0.72 mM apo R2-W48F/D84E (in 100 mM Na-Hepes, pH 7.6) and 2.5 mM $FeSO_4$ (in 5 mN H_2SO_4) were mixed at 5 °C, and the mixture was allowed to age for 0.83 s prior to being mixed with 0.5 equivalent volume of either 30 mM sodium dithionite (dashed trace) or O_2-free Na-Hepes buffer (solid trace). Alternatively, the reaction solution from the first mix was aged for 120 s prior to being mixed with dithionite (dotted trace). In each case, the protein was rapidly (after ~1 min reaction time) desalted, as described in Materials and Methods, and then incubated on ice to allow for conversion to the purple complex.

mm/s is lost. The subtraction result of spectra of the brown and purple species acquired with a strong (8 T) applied field demonstrates that the decaying Fe(III) species are diamagnetic (Figure S2, Supporting Information). Because the two major decaying doublets are of equal intensity, have parameters characteristic of high-spin Fe(III) ions, and arise from diamagnetic species, they are almost certainly associated with an antiferromagnetically coupled diiron(III) cluster in which the individual Fe(III) ions have different Mössbauer parameters (as is the case for the normal μ-oxodiiron(III) cluster in wild-type R2). The parameters of these two Fe(III) ions are similar to those of the normal μ-oxodiiron(III) cluster. Most revealingly, the large values of ΔE_Q strongly suggest the presence of an oxo bridge. The paramagnetic features that develop may be analyzed as originating from a single slowly relaxing high-spin Fe(III) site with a small value of the zero-field parameter, D ($|D| \sim 0.5$ cm^{-1}).[55-57] The fractional area undergoing change in the brown-to-purple transition was observed to vary significantly (18 ± 4 and 32 ± 4% in two trials), but was closely correlated with A_{550} at completion. Under the assumption that the absorption area undergoing change reflects the quantity of the purple diiron(III)−phenolate product formed, one would calculate that 0.5 equiv (32% × 3.1 equiv of Fe ÷ 2 Fe/product = 0.5 equiv of product) was formed in the sample of Figure 10. By comparison of this value with the optical absorption data, one would calculate $\epsilon_{550} = 4200 \pm 600$ M^{-1} cm^{-1}. The precise agreement of this value with that calculated from the GC/MS data validates the assumptions used in both calculations. The

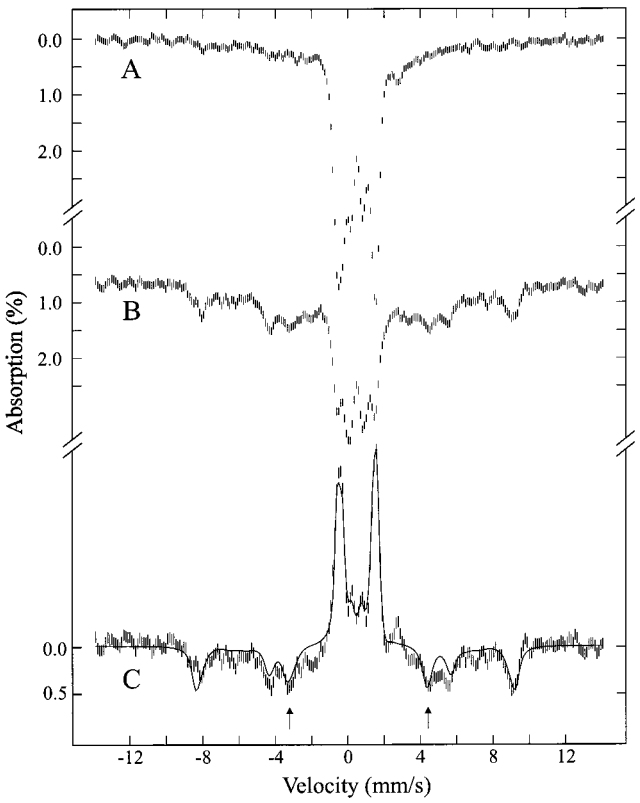

Figure 10. Mössbauer spectra of products from the reaction at 5 °C of apo R2-W48F/D84E with Fe(II) and O_2 frozen 1 min (A) or 48 h (B) after initiation of the reaction. The spectra are from the same sample, which was initially frozen after 1 min and characterized completely by Mössbauer, then thawed and incubated on ice for 48 h prior to re-freezing and re-characterization. The reaction conditions are given in the legend to Figure 2. Both spectra were recorded at 4.2 K with a field of 50 mT applied parallel to the γ-beam. Spectrum C was generated by subtracting spectrum A from spectrum B. The features pointing upward are associated with the species that convert into the purple complex, whereas the downward features are associated with the purple complex itself. The solid line plotted over the data in part C is a simulation of the difference spectrum. The decaying features were simulated as three quadrupole doublets with the following parameters: $\delta(1) = 0.52$ mm/s, $\Delta E_Q(1) = 2.20$ mm/s, 14%; $\delta(2) = 0.55$ mm/s, $\Delta E_Q(2) = 1.72$ mm/s, 14%; and $\delta(3) = 0.48$ mm/s, $\Delta E_Q(3) = 0.54$ mm/s, 3%. The developing paramagnetic features were simulated with the following parameters: $S = {}^5/_2$, $D = -0.5$ cm^{-1}, $E/D = {}^1/_3$, $\delta = 0.55$ mm/s, $\Delta E_Q = -0.5$ mm/s, $\eta = -3$ $A/g_n\beta_n = (-215, -222, -228)$ kG. The paramagnetic features are plotted at an intensity corresponding to 26% of the total. The arrows in spectrum C indicate the peaks from the excited state (see text).

(55) Although the paramagnetic features that develop can be analyzed as originating from a single site, they must be associated with two Fe ions, as they are the only features to develop upon decay of diamagnetic diiron(III) precursors. On the basis of this conclusion, which is consistent with the crystal structure, we have analyzed the paramagnetic Mössbauer component by assuming that it arises from two adjacent Fe(III) ions. Preliminary analysis indicates that coupling between the Fe(III) ions must be extremely weak. A coupling interaction (exchange or dipolar) between the two Fe(III) ions would be expected to affect the paramagnetic Mössbauer component in the following way. Electronic states that would in a completely uncoupled system exhibit isotropic spin expectation values (e.g., the first excited Kramers' doublet) would be perturbed by the coupling such that their expectation values would no longer be isotropic. As a consequence, Mössbauer peaks from these states would be broadened and their field-orientation dependencies diminished with increasing magnitude of $|J|$. To the contrary, the peaks at −3.25 and +4.45 mm/s (marked by arrows in Figure 10), which originate from the first excited Kramers' doublet, are quite sharp and show a dependence on the orientation of the applied field relative to the γ-beam, as expected for an isotropic doublet (ref 56). From simulations of the spectra according to our present understanding we conclude that $|J|$ must be less than ~10^{-4} cm^{-1} to account for the data. This weak interaction seems incompatible with the expected ~3.4 Å separation of the Fe(III) ions, for which dipolar couplings on the order of 10^{-2} cm^{-1} would be expected (ref 57). Thus, the paramagnetic features associated with the purple Fe(III)−phenolate complex are not yet satisfactorily explained. Nevertheless, we tentatively conclude that the features reflect two Mössbauer-indistinguishable and essentially uncoupled Fe(III) sites.

(56) The paramagnetic feature must have $E/D = {}^1/_3$, as the EPR spectra of the purple samples show the characteristic $g = 4.3$ signal, and this signal forms concomitantly with the 550-nm absorption.

(57) Bencini, A.; Gatteschi, D. *EPR of exchange coupled systems*; Springer: Berlin, Germany, 1990.

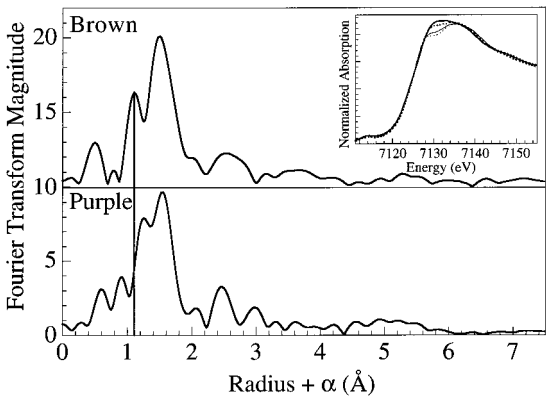

Figure 11. Fourier transforms of EXAFS data for representative brown (top frame) and purple (bottom frame) samples. The vertical line at 1.2 Å marks the short 1.75 Å Fe−O distance in the brown sample and indicates that this feature disappears upon conversion to the purple species. The inset shows the X-ray absorption near edge spectra for four product samples: wild-type R2, R2-D84E, brown R2-W48F/D84E, and purple R2-W48F/D84E. All of the edges are superimposed at an energy characteristic of Fe(III). A dip in the edge at 7130 eV is seen in the samples with short Fe−O distances (wild-type, thinner dotted line; R2-D84E, thinner solid line; brown R2-W48F/D84E, thicker dotted line).

Table 3. EXAFS First Shell Fitting Analysis

	Fe−O			Fe−O				
model	R (Å)	cn	$\sigma^2 \times 10^3$	R (Å)	cn	$\sigma^2 \times 10^3$	F	ϵ'
Brown: FT from 1 to 13 Å^{-1}; Backtransform from 0.95 to 1.95 Å								
O	2.01	3	2.8				0.717	0.0918
O, O	1.75	1	1.9	2.00	5	6.2	0.523	0.0760
Purple: FT from 1 to 14 Å^{-1}; Backtransform from 1.0 to 1.90 Å								
O	1.98	5	9.6				0.497	0.0457
O, O	1.97	4	7.7	2.08	1	5.8	0.447	0.0588

simplest interpretation of the observed conversion of diamagnetic diiron(III) species to paramagnetic diiron(III) species is that a bridging ligand that mediates efficient antiferromagnetic exchange coupling in the brown product is lost upon conversion to the purple Fe(III)−phenolate species. This conclusion is consistent with the crystallographic data indicating that the Fe ions in the purple complex are bridged only by carboxylates, which are poor mediators of electron exchange. Given the aforementioned large ΔE_Q values of the decaying Fe(III) species, the most obvious candidate for the displaced bridging ligand is a μ-oxo.

The conclusion that the brown-to-purple conversion involves a redox-neutral ligand rearrangement that includes the loss of a μ-oxo is supported by the X-ray absorption spectra of both species. Comparison of the Fe absorption edges for the brown and purple samples with those for the diiron(III) forms of wild-type R2 and R2-D84E (Figure 11, inset) reveals no significant differences in the edge energies, confirming the conclusion from the Mössbauer data that all (or at least the vast majority) of the Fe in the inhomogeneous brown and purple samples is in the III oxidation state. Filtered first shell fits to data from four different brown samples all indicate the presence of a short Fe−O vector. For the brown samples that, after incubation, gave the highest yield of purple species (0.5 equiv on the basis of the change in the Mössbauer spectrum), the average Fe−O distances are 1.75 ±.0.01 and 2.00 ± 0.01 Å (Table 3). For the brown sample with the lowest percentage of reactive species (18%), the shorter of the two refined distances is skewed to 1.87 Å, suggesting that the short Fe−O interaction is associated with the reactive species rather than with the other Fe(III) species in the heterogeneous samples. In the data for the four purple samples, the first shell is statistically best modeled with a single shell of Fe−O/N scatterers at 1.99 ±.0.01 Å (Table 3). If the purple samples' first shells are modeled with two Fe−O/N interactions, the short Fe−O distances refine to 1.95 ± 0.03 Å and the longer distances refine to 2.06 ± 0.02 Å. Thus, the short Fe−O interaction detected in the brown product is no longer detectable after conversion to the purple complex. The loss of this interaction can be seen clearly in the Fourier transform of the EXAFS data (Figure 11).

Discussion

Rationale for Reprogramming R2 into a Monooxygenase. Reaction of the diiron(II) form of wild-type *E. coli* R2 with O_2 results in rapid accumulation of a stoichiometric quantity of the one-electron oxidized (formally Fe(IV)Fe(III)) cluster **X**,[32,46,58−62] which can generate the tyrosyl radical (Y122•) by one-electron oxidation of Y122 as it converts to the product μ-oxodiiron(III) cluster.[46,63,64] The oxidation state of **X** and the fact that it precedes Y122• in the reaction sequence imply that the "extra" electron, which is required to balance the four-electron reduction of O_2 with the 3 electrons obtained by conversion of the diiron(II)-Y122 reactant to the diiron(III)-Y122• product, is transferred to the cluster during formation of **X**. Stoichiometry measurements indicate that this electron can be provided by excess Fe(II) in solution or exogenous reductants such as ascorbate.[46,65−67] Attempts to expose the two-electrons-oxidized diiron precursor(s) to **X** by carrying out the reaction with limiting Fe(II) in the absence of reductant to slow the electron injection step resulted instead in the detection of a transient tryptophan cation radical ($W^{+\bullet}$) on the protein.[6,63,68] More recent results have shown that the $W^{+\bullet}$ forms concomitantly with **X** without significant accumulation of prior intermediates, and that the $W^{+\bullet}$ is efficiently reduced by a variety of one-electron donors.[6] X-ray crystallographic characterization of R2 identified the near-surface residue, W48, which is connected to the buried diiron cluster by a hydrogen bond chain involving D237 and Fe1 ligand H118, as the most likely site of the $W^{+\bullet}$,[8] and recent experiments have confirmed that electron transfer to the cluster is blocked by substitution of this residue with F.[7,69] These results suggest that the network involving W48 functions to split the two oxidizing equivalents of an early diiron intermediate by shuttling 1 equiv to the surface of the protein (the $W^{+\bullet}$), where it can be efficiently quenched by an exogenous

(58) Bollinger, J. M., Jr.; Stubbe, J.; Huynh, B. H.; Edmondson, D. E. *J. Am. Chem. Soc.* **1991**, *113*, 6289−6291.
(59) Sturgeon, B. E.; Burdi, D.; Chen, S.; Huynh, B. H.; Edmondson, D. E.; Stubbe, J.; Hoffman, B. M. *J. Am. Chem. Soc.* **1996**, *118*, 7551−7557.
(60) Willems, J.-P.; Lee, H.-I.; Burdi, D.; Doan, P. E.; Stubbe, J.; Hoffman, B. M. *J. Am. Chem. Soc.* **1997**, *119*, 9816−9824.
(61) Burdi, D.; Willems, J.-P.; Riggs-Gelasco, P.; Antholine, W. E.; Stubbe, J.; Hoffman, B. M. *J. Am. Chem. Soc.* **1998**, *120*, 12910−12919.
(62) Burdi, D.; Sturgeon, B. E.; Tong, W. H.; Stubbe, J.; Hoffman, B. M. *J. Am. Chem. Soc.* **1996**, *118*, 281−282.
(63) Bollinger, J. M., Jr.; Edmondson, D. E.; Huynh, B. H.; Filley, J.; Norton, J. R.; Stubbe, J. *Science* **1991**, *253*, 292−298.
(64) Tong, W. H.; Chen, S.; Lloyd, S. G.; Edmondson, D. E.; Huynh, B. H.; Stubbe, J. *J. Am. Chem. Soc.* **1996**, *118*, 2107−2108.
(65) Ochiai, E.; Mann, G. J.; Gräslund, A.; Thelander, L. *J. Biol. Chem.* **1990**, *265*, 15758−15761.
(66) Elgren, T. E.; Lynch, J. B.; Juarez-Garcia, C.; Münck, E.; Sjöberg, B.-M.; Que, L., Jr. *J. Biol. Chem.* **1991**, *266*, 19265−19268.
(67) Miller, M. A.; Gobena, F. T.; Kauffmann, K.; Münck, E.; Que, L., Jr.; Stankovich, M. T. *J. Am. Chem. Soc.* **1999**, *121*, 1096−1097.
(68) Bollinger, J. M., Jr.; Tong, W. H.; Ravi, N.; Huynh, B. H.; Edmondson, D. E.; Stubbe, J. *J. Am. Chem. Soc.* **1994**, *116*, 8024−8032.
(69) Schmidt, P. P.; Rova, U.; Katterle, B.; Thelander, L.; Gräslund, A. *J. Biol. Chem.* **1998**, *273*, 21463−21472.

Scheme 1. Reaction Sequence Leading to Formation of the Purple Fe(III)−Phenolate Complex in R2-W48F/D84E

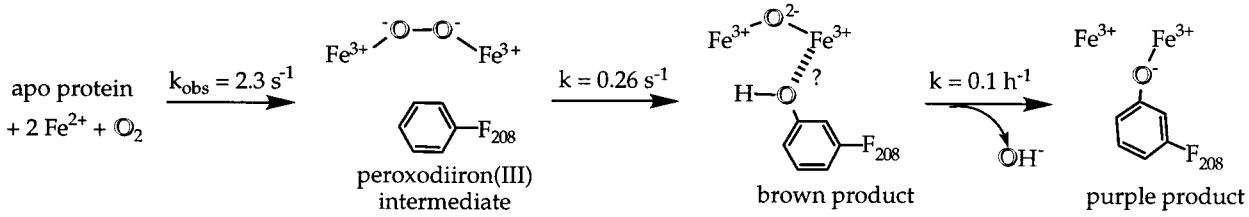

reductant. The second equivalent is retained on the buried diiron cluster (**X**) for conversion of Y122 to the radical.

The probable importance of this structural adaptation for directing the mechanism (and therefore the outcome) of the R2 reaction is emphasized by contrast with the mechanism of O_2 activation in MMOH, which lacks a comparable hydrogen bond chain between the diiron cluster and a near-surface tryptophan.[11] The MMOH reaction proceeds sequentially through the peroxodiiron(III) complex **P** and the formally diiron(IV) complex **Q**, which are both more oxidized than the product diiron(III) cluster by *two* electrons.[4,70−76] Thus, the absence of the electron-transfer step in MMOH allows two-electron-oxidized diiron species to persist, and a two-electron-oxidation outcome (hydroxylation) results. On the basis of this information alone, one might postulate (1) that the most crucial distinction between the R2 and MMOH reaction mechanisms is the electron-transfer step and (2) that the primary structural determinant of their divergent outcomes is the presence or absence of the electron-shuttling H-bond chain. Indeed, it was recently shown that such "outer sphere" control *can* be sufficient to distinguish hydroxylation from tyrosyl radical production in the O_2 reaction of the aforementioned R2-F208Y protein.[5] This reaction actually partitions between Y208 hydroxylation and Y122$^\bullet$ formation.[24] The former predominates under standard reaction conditions (as noted above), but the partition ratio can be influenced in favor of the latter by inclusion of a facile one-electron reductant such as ascorbate.[5] Disruption of the H-bond chain by the W48F substitution renders Y208 hydroxylation the exclusive outcome, even in the presence of high concentrations of ascorbate. Thus, at 0.11 M ascorbate, R2-F208Y effects primarily one-electron oxidation of Y122 while R2-W48F/F208Y effects almost exclusively Y208 hydroxylation.[5] These results seem to validate the notion that the network involving W48 might be sufficient to distinguish the wild-type R2 mechanism and outcome from that of a monooxygenase.

However, recent kinetic and spectroscopic characterization of O_2 activation by R2-W48F suggests that control of the reaction by the protein is multifactorial.[7] The rapid accumulation of a coupled diradical intermediate containing both **X** and Y122$^\bullet$ (hereafter denoted **X**-Y$^\bullet$) implies that Y122$^\bullet$ is produced in the mutant protein at an earlier step in the mechanism. Rather than obtaining the "extra" electron via W48 (as occurs in wt R2), the precursor to **X** abstracts an electron directly from Y122. The Y122 radical is produced 10-fold more rapidly by this altered mechanism than by **X** in the normal mechanism.[7] This result underscores the considerable reactivity of the **X** precursor toward one-electron reduction. Furthermore, kinetic evidence implies that the **X** precursor accumulates. Although technical difficulties have thus far thwarted its unambiguous spectroscopic characterization, it lacks the absorption signatures of MMOH intermediates **P** and **Q**.[7] On the bases of the hypothesis that the W48 chain is solely responsible for distinguishing the R2 mechanism from that of MMOH and the assumption that the W48F substitution affects only the electron-transfer step, one would have predicted that a **Q**-like species would accumulate in R2-W48F. One possible interpretation of the observation to the contrary is that the R2 cluster is "tuned" to form an intermediate that is structurally distinct from the MMOH intermediates and inherently more reactive toward one-electron reduction. Such tuning would most likely result from differences in the coordination sphere of the R2 diiron(II) cluster relative to the MMOH reactant cluster.

In contemplating possible structural bases for this tuning, we noted (as others did before) that there is a single nonidentity among the amino acid iron ligands of R2 and MMOH: the counterpart of R2 ligand D84 is E114 in MMOH.[8,9,11,12,15] Each of these is monodentate to a single Fe ion in the diiron(II) form of the protein and extends away from the cluster roughly along the Fe− Fe axis. Perhaps partly as a consequence of the extra methylene unit in the MMOH ligand, the Fe− Fe distance in its diiron(II) form is 0.6 Å shorter than that in R2 (3.3 Å in MMOH versus 3.9 Å in R2), as determined from crystallographic studies on the two proteins.[12,28] In light of recent evidence for marked changes in this distance during the reaction sequences of both proteins,[42,74] we postulated that the "linker length" of this carboxylate ligand might be important for tuning the reactivity of the clusters. To test this notion, we replaced D84 with E in *E. coli* R2. Nearly 1 equiv of a relatively slowly decaying ($t_{1/2} \sim 0.7$ s at 5 °C) μ-1,2-peroxodiiron(III) complex, which has spectroscopic properties similar to those of MMOH **P**, was shown to accumulate upon reaction of O_2 with the diiron(II) protein.[2] Subsequent crystallographic characterization of reduced R2-D84E revealed that several adjustments in coordination render its diiron(II) cluster more similar to that in reduced MMOH than to that in reduced wt R2.[29] Despite this greater structural and mechanistic similarity to MMOH, R2-D84E does not effect a monooxygenase outcome: the variant protein still generates 1.1 ± 0.1 equiv of Y122$^\bullet$ (compared to 1.2 ± 0.1 equiv in wt R2) upon reaction of its diiron(II) form with O_2.[2] On the basis of this result, we reasoned that D84 and W48 may function somewhat redundantly in control of O_2 activation, and correctly predicted that a hydroxylation outcome might occur if the MMOH **P**-like intermediate were made to accumulate in an R2 variant also defective in the electron injection step.

Summary of the Mechanism of the R2-W48F/D84E Reaction. The combined chemical, kinetic, and spectroscopic data on the R2-W48F/D84E reaction support the pathway

(70) Lee, S.-K.; Nesheim, J. C.; Lipscomb, J. D. *J. Biol. Chem.* **1993**, *268*, 21569−21577.
(71) Lee, S.-K.; Fox, B. G.; Froland, W. A.; Lipscomb, J. D.; Münck, E. *J. Am. Chem. Soc.* **1993**, *115*, 6450−6451.
(72) Liu, K. E.; Valentine, A. M.; Wang, D.; Huynh, B. H.; Edmondson, D. E.; Salifoglou, A.; Lippard, S. J. *J. Am. Chem. Soc.* **1995**, *117*, 10174−10185.
(73) Nesheim, J. C.; Lipscomb, J. D. *Biochemistry* **1996**, *35*, 10240−10247.
(74) Shu, L. J.; Nesheim, J. C.; Kauffmann, K.; Münck, E.; Lipscomb, J. D.; Que, L., Jr. *Science* **1997**, *275*, 515−518.
(75) Valentine, A. M.; Stahl, S. S.; Lippard, S. J. *J. Am. Chem. Soc.* **1999**, *121*, 3876−3887.
(76) Lee, S.-K.; Lipscomb, J. D. *Biochemistry* **1999**, *38*, 4423−4432.

illustrated in Scheme 1. The MMOH **P**-like peroxodiiron(III) intermediate accumulates in near stoichiometric yield, and one significant pathway for its decay leads to incorporation of one of its oxygen atoms at the ϵ-position of F208. We propose that, in this pathway, the second peroxide O-atom of the intermediate becomes a μ-oxo ligand. The basis for this hypothesis is 2-fold. First, it has been shown that the oxo bridge in the diiron(III) cluster of R2-Y122F originates from O_2.[27] Second, the Mössbauer and EXAFS data in this work, when considered with extensive model studies,[77,78] provide strong evidence for the presence of a μ-oxo in the brown product. The primary species that decays in the transition to the purple product contains high-spin Fe(III), is diagmagnetic, and has large quadrupole splitting parameters (1.72 and 2.15 mm/s). These characteristics, when they are associated, are unmistakable hallmarks of the μ-oxo-diiron(III) unit. (For comparison, the ΔE_Q values for the two resolved Fe sites of the diamagnetic μ-oxodiiron(III) cluster in wild-type R2 are 1.6 and 2.4 mm/s.[17,46,79]) Even more definitively, the Fe−O distance of 1.75 Å measured by EXAFS is slightly shorter than the Fe−μ-oxo distance found for wt R2 (1.80 Å[42]) and is identical with that found for oxidized R2-D84E (not shown), in which previous crystallographic studies clearly revealed the presence of a μ-oxo.[29] It is somewhat noteworthy that this short Fe−O interaction can even be detected in the brown R2-W48F/D84E samples, given that meaningful EXAFS characterization of heterogeneous samples is notoriously difficult. Two factors make this detection possible. First, EXAFS spectra of diiron complexes are remarkably sensitive to the presence of these short μ-oxo interactions.[78] Second, potentially interfering first shell interactions at short distances are apparently absent in the remaining Fe in the heterogeneous brown samples.

To complete the pathway in Scheme 1, the initial μ-oxo-containing (brown) species, in which the phenolic O-atom may or may not be weakly coordinated by Fe2, reacts very slowly to lose of its O-atom bridge as the phenolic proton is lost and the phenolate coordinates to Fe2. This step rationalizes the conversion of a diamagnetic diiron(III) species into a paramagnetic species observed by Mössbauer and the loss of the short Fe−O interaction observed by EXAFS. This scheme is also consistent with results from previous studies on the R2 protein and variants thereof. For example, the product cluster in the self-hydroxylated R2-Y122F/E238A protein was shown by X-ray crystallography to have a structure with marked similarities to that proposed for the initial brown product of the R2-W48F/D84E reaction.[26] An O-atom bridge (of undetermined protonation state) *was* observed, and an Fe−$O_{phenolate}$ distance of 2.8 Å was reported (compared to 2.38 Å in the present structure). This somewhat long Fe−$O_{phenolate}$ distance in R2-Y122F/E238A was interpreted as a reflection of a protonated (neutral) phenol weakly coordinated to Fe2. Consistent with this notion, no phenolate-to-Fe(III) charge-transfer band was observed. Only a weak feature at 490 nm, very similar to the feature exhibited by the initial brown product of the R2-W48F/D84E reaction, was detected.[26] The striking analogy between the structurally characterized R2-Y122F/E238A product and the brown R2-W48F/D84E product lends additional credence to our hypothesis concerning the nature of the brown-to-purple transition. In addition, the proposal of a complex ligand rearrangement can rationalize the extreme sluggishness of the brown-to-purple transition. This rearrangement should require coupled deprotonation of the phenol oxygen, protonation of the bridging ligand, net displacement of the bridging ligand by the phenolate, and perhaps release of the displaced ligand as hydroxide or water. Even the much simpler exchange of the oxo bridge with solvent is quite slow, requiring several minutes in both wt R2 and R2-Y122F.[80]

It is clear that the substoichiometric yield of ϵ-hydroxyphenylalanine in the R2-W48F/D84E reaction reflects the existence of alternative pathways for decay of the peroxo intermediate.[81] Among these pathways, a minor one leads to formation of a small quantity of Y122$^{\bullet}$. This pathway presumably involves conversion of the intermediate to the diiron(III) product(s) by sequential one-electron reduction steps. Other pathways involving initial one-electron reduction of the peroxo species (or some isoelectronic successor) might also be anticipated. It is therefore noteworthy that no evidence for accumulation of an **X**-like species (**X** is one-electron more reduced than the peroxo complex) is observed in the Mössbauer spectra of the freeze-quenched samples. Thus, if the alternative mechanistic pathways involve a diiron species that is isoelectronic with **X**, this species must either have significantly different Mössbauer characteristics or decay rapidly relative to its formation (so as not to accumulate). By contrast, every R2 variant with the wt iron ligands that we have studied in detail (including the wt protein, R2-W48F, R2-Y122F, and R2-W48F/Y122F) accumulates a significant quantity of **X** in its reaction sequence.[7,46,63,82]

Possible Mechanistic Implications of the D84E Requirement for F208 Hydroxylation. The observation of differences in the products and the accumulating intermediates of the R2-W48F and R2-W48F/D84E reactions underscores the existing uncertainty regarding the importance of subtle adjustments in cluster coordination for the divergent control of O_2 activation by R2 and the other diiron−carboxylate proteins. The popular presumptions that the R2 cluster with its wild-type ligands reacts with O_2 to form the MMOH **P**-like μ-1,2-peroxodiiron(III) complex[21,53,83] and that the mechanism is subsequently distinguished from that of MMOH by the electron-transfer step imply that the subtle differences in cluster coordination that are observed in these two proteins are of (at most) secondary functional importance. Subscribing to these presumptions, one might mistakenly have expected the electron-transfer-disabling W48F substitution to be sufficient to change the reaction outcome. One possible interpretation of the present results to the contrary, which could rationalize both the D84E requirement for F208 hydroxylation and the accumulation of **X** in R2 proteins with the wild-type ligands but not in R2 proteins with the D84E substitution, is that the structure of the R2 cluster with its wild-type ligand set favors formation of an adduct that is distinct in structure and reactivity from the peroxodiiron(III) complex that accumulates in both MMOH and R2-D84E. In the absence of definitive experimental evidence that an equivalent peroxo complex is an intermediate in the reaction of wild-type R2 or

(77) Kurtz, D. M. *Chem. Rev.* **1990**, *90*, 585−606.

(78) Hedman, B.; Co, M. S.; Armstrong, W. H.; Hodgson, K. O.; Lippard, S. J. *Inorg. Chem.* **1986**, *25*, 3707−3711.

(79) Lynch, J. B.; Juarez-Garcia, C.; Munck, E.; Que, L., Jr. *J. Biol. Chem.* **1989**, *264*, 8091−8096.

(80) Backes, G.; Loehr, T. M.; Sjöberg, B.-M.; Sahlin, M.; Sanders-Loehr, J. *Biochemistry* **1989**, *28*, 1923−1929.

(81) One conceivable alternative pathway for decay of the peroxo species would lead to ζ-hydroxylation of F208. This outcome would escape our detection if the resulting tyrosine were (due to geometric constraints) unable to coordinate strongly to the diiron cluster to produce an RR-active species. Thus, the possibility remains that F208 hydroxylation is the vastly predominant outcome of the reaction, with both ϵ- and ζ-derivatives being formed in comparable yield. This possibility could be tested by GC/MS analysis of product samples prepared with $^{18}O_2$. In this case, tyrosine produced by ζ-hydroxylation of F208 would co-chromatograph with the other tyrosines in the protein but would have two units greater mass.

(82) Bollinger, J. M., Jr., 1993, Ph.D. Thesis, Massachusetts Institute of Technology.

(83) Stubbe, J.; Riggs-Gelasco, P. *TIBS* **1998**, *23*, 438−443.

that the peroxo complex that accumulates in D84E variants is chemically and kinetically competent to produce **X**, this hypothesis remains viable.

Acknowledgment. We thank Daniel Jones, Director of the Mass Spectrometry Facility at Pennsylvania State University, for the GC/MS analysis. This work was supported by NIH grants GM55365 (J.M.B), GM47295 (B.H.H.), and GM18865 (T.M.L.), by funds from the Robert H. Lurie Cancer Center at Northwestern University (A.C.R.), the Searle Scholars Program of the Chicago Community Trust (J.M.B.), and the Camille and Henry Dreyfus Foundation (New Faculty Award to J.M.B. and Faculty Start-up Grant for Undergraduate Institutions to P.J.R.-G.). Funds for the resonance Raman spectroscopy instrumentation at OGI were provided by the NSF (BIR-9216592). Stanford Synchrotron Radiation Laboratory (SSRL) is funded by the Department of Energy, Office of Basic Energy Sciences, and the DND-CAT Synchrotron Research Center at the Advanced Photon Source is supported by the E.I. DuPont de Nemours & Co., The Dow Chemical Company, the NSF, and the State of Illinois.

Supporting Information Available: Figure S1 depicting quantitative analysis of the Mössbauer spectrum of the brown product and Table S1 giving Mössbauer paramaters of component subspectra from this analysis and Figure S2 showing the subtraction result of the Mössbauer spectra of brown and purple species acquired with a strong (8 T) applied field (PDF). This material is available free of charge via the Internet at http://pubs.acs.org.

JA002114G